DOI: 10.1111/cgf.12752
Pacific Graphics 2015
N. J. Mitra, J. Stam, and K. Xu
(Guest Editors)

*Volume 34 (2015), Number 7*

# Quadratic Contact Energy Model for Multi-impact Simulation

Tianxiang Zhang [1] Sheng Li [1†] Dinesh Manocha [2] Guoping Wang [1‡] Hanqiu Sun [3]

[1]Peking University [2]University of North Carolina at Chapel Hill [3]Chinese University of HongKong

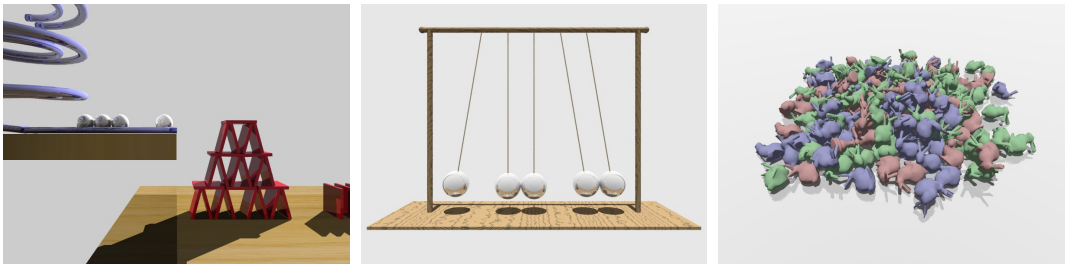

(a) (b) (c)

**Figure 1:** *Our algorithm is able to simulate various scenarios: (a) a Rube Goldberg machine composed of several parts; (b) simulation of wave propagation in Newton's Cradle; (c) many bunnies and pawns falling on the ground.*

**Abstract**

*Simultaneous multi-impact simulation is a challenging problem that frequently arises in physically-based modeling of rigid bodies. There are several physical criteria that should be satisfied for rigid body collision handling, but existing methods generally fail to meet one or more of them. In order to capture the inner process of potential energy variation, which is the physical foundation of collisions in a multi-impact system, we present a novel* quadratic contact energy *model for rigid body simulation. By constructing quadratic energy functions with respect to the impulses, post-impact reactions of rigid bodies can be computed efficiently. Our model can satisfy the physical criteria and can simulate various natural phenomena including the* wave effect. *Also, our model can be easily combined with Linear Complementary Problem (LCP) and can provide feasible results with any restitution coefficient. In practice, our model can solve the simultaneous multi-impact problem efficiently and robustly, and we highlight its performance on different benchmarks.*

## 1. Introduction

Modeling multi-body impact is a widely researched problem in rigid body simulation. The collision process generally consists of two stages, contact, compression and decompression, and can hardly be simulated with only a discrete configurations of the bodies. For this reason, impacts between rigid bodies are treated as happening in an instant in many widely-used simulation models. However, with this assumption, determining the sequence of impacts becomes an ill-posed problem. Simultaneity and propagation are two categories of models used when referring to the sequencing problem. Simultaneity models assume all the impacts occur at the same time instance and should be solved simultaneously. Propagation models assume that the impacts happen sequentially and a pairwise propagated method should be applied to resolve them.

† Correspondence author, lisheng@pku.edu.cn
‡ Correspondence author, wgp@pku.edu.cn

In computer graphics, simultaneity and propagation models have different applications, but each of them has some limitations. Smith et al. [SKV*12] discuss the advantages and disadvantages of both type of models and propose five physical desiderata for a correct algorithm for instantaneous impact: **Break away** (BRK), **Symmetry preserved** (SYM), **Energy bounded** (KIN), **Momentum conserved** (MOM) and **One-sided impulses** (ONE).

Linear complementary problem (LCP) is one of the moost widely used dynamics model. However, it fails to satisfy (BRK), and cannot work for *Newton's Cradle*, because post-impact relative velocities are incorrectly computed due to incorrect predictions from pre-impact relative velocities. For example, if the pre-impact relative velocity equals zero, the post-impact relative velocity will remain zero even if a non-zero impulse is applied. This is inconsistent with real-world experiments and therefore, not suitable for multi-impact systems. In order to deal with (BRK), some improvements have been proposed for LCP. Smith et al. [SKV*12] proposed *Generalized Reflection* (GR), making it possible to simulate breaking away phenomena while preserving the symmetry and bounding the energy.

The effect of breaking away is actually caused by the propagation of a shock wave in the chain of objects, which is the physical basis of collisions in nature [SHB*08]. In order to describe this phenomenal, we propose **Wave effect** (WAV) as the physical criteria for accurate multi-body simulation.

(WAV) **Wave effect.** Theoretically, wave effect refers to the propagation of shock waves through contacting bodies at the time of collision. Therefore, the post-impact relative velocity of a contact point should not only be determined by its pre-impact velocity locally, but also influenced by other contact points. This is due to the fact that momentum and energy also propagate along with the wave in a chain of bodies [SHB*08]. If this propagation effect is ignored, the influence of other contact points is being ignored during the computation. As a result, its post-impact relative velocity will be computed relative to the pre-impact velocity and may not be accurate. The (BRK) effect in *Newton's Cradle* is a typical case of wave propagation. The wave effects can be observed in physical experiments [Pay08], e.g. colliding balls shown in Fig. 2, where two balls on each side should exchange their velocities after the impact, while the ball in the middle will remain stable.

However, due to the complexity of multiple impacts, analyzing the wave in detail during an impact is either considered expensive or unnecessary in prior approaches. Therefore, the physical rules corresponding to (WAV) cannot be satisfied, and this may result in simulation artifacts.

**Contributions**: We present a *Quadratic Contact Energy* (QCE) model for rigid multiple body simulation. Our model satisfies all the above physical desiderata as well as (WAV).

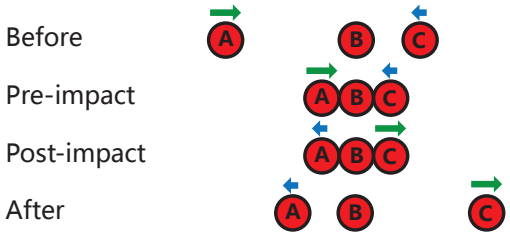


**Figure 2:** *Velocity exchange caused by wave effect during the rigid contact. Impacts occur among three identical balls. After the impact, ball A and C should exchange their velocities. This phenomenon can be observed in real-world experiments [Payr 2008].*

The accurate wave propagation during an impact can be captured by resolving the QCEs. We analyze the contacts and model the potential energy of each contact point with QCE, there making the simulation of rigid objects more accurate. Moreover, the equation of QCE can be solved analytically without either numerical errors or large computational overhead.

## 2. Related Work

In order to model the law of multiple impacts in rigid body dynamics, various models have been proposed in computer graphics and mechanics [Hah88, Bar89, CR98, Bro99, MC95]. Some of these have been further improved or substituted, e.g. models of the velocity-impulse level replace those of force-acceleration level [AP97]. Each of these models has unique advantages in some simulation scenarios while they fall short in others. None of them are totally robust or produce the correct outcome in all cases. A recent survey of these simulation models is given in [BET14].

Generally, LCP is the most widely used model [Bar89, Bar91, Ste00], and it computes plausible reactions after an impact in most cases. It converts the rigid body dynamics into a linear complementary problem by applying the Signorini Condition. The linear problem can be solved using numerical methods [NE15]. Projected Gauss-Seidel(PGS) is one typical solver [Mur88, Erl04]. PGS can generate feasible results within a few iterations in most cases. Recently, Gauss-Siedel based splitting method has also been used [TBV12]. This method improves the convergence and parallelism.

LCP itself has various formulations [WLN*13]. When used in computer graphics, the typical LCP formulation has some limitations. For example in *Newton's Cradle*, the phenomenon of breaking away is expected. However LCP will generate an unreal sticking result [Bar89, SKV*12]. This is caused by its intrinsic formulation. To solve this problem, Smith et al. [SKV*12] proposed the Generalized Reflection(GR), which combines LCP with propagation ap-

proaches. Other research focuses on the sequence of contacts to improve the stability and performance [GBF03, Erl07].

Impacts of rigid bodies have also been extensively studied in engineering mechanics. The relationship between local deformation and contact impulse during a collision has been studied in contact mechanics [SH96]. The micro force-indentation law can also be applied to complex multi-impact systems [KS87, LN90, LN94, LZB08]. Poisson hypothesis is combined with LCP in order to compute accurate restitution impulse [AP97]. With the Hertz contact model or other models, a set of second-order differential equations can be used to represent the behavior of each body in the system. Apart from contact mechanics, shockwaves in a chain of beads during a collision have been shown to reveal the contact law of rigid bodies [HHL99, SM01, JMSS07, NB14].

## 3. Potential Energy Analysis and Modeling

The wave effect is widely observed and studied in engineering mechanics. In order to analyze its propagation over a very short time duration, a collision is treated as a process, instead of as an instant event. This is somewhat similar to the quasi-rigid objects simulation in [PPG04]. Under the effect of local deformation, a body's velocity varies over the time duration. Through the variation of the velocity, shock wave propagates through the bodies. Therefore the wave effect can be easily simulated by analyzing the velocity variations of bodies. Our formulation is inspired by these observations.

Deformable objects undergo significant deformation during the collision. Therefore Finite Element Method (FEM) or other methods are used to analyze the shape of deformation. Once the elastic modulus becomes infinite, a deformable body turns into a rigid body and the local deformation becomes infinitely small. In this case, the deformation cannot be simulated directly by FEM. Therefore, in order to analyze the process during the contact of rigid bodies, the micro-deformation is simulated indirectly based on its potential energy, instead of analyzing its shape.

In terms of positive or negative relative velocity, the collision process can be decomposed into two phases: the compression phase and the expansion phase. Local deformation, which contains potential energy and provides contact force, exists in both the phases. The potential energy of a contact point has positive correlation to the local deformation. Starting from zero, the potential energy increases during the compression phase and decreases during the expansion phase. Returning to zero indicates the end of contact at this point. Therefore, we use the potential energy of each contact point as the key to model a multi-impact system.

Considering a system having $n$ rigid bodies with generalized position coordinates $\mathbf{q} \in \mathbb{R}^{6n}$ and the mass matrix $\mathbf{M} \in \mathbb{R}^{6n\times 6n}$. Let us assume that in this system $m$ contact points are detected. For an arbitrary contact point $i$, the potential energy of this point $\mathbf{E}_i$ can be represented by the negative work done by contact force $\mathbf{f}_i$ and its relative velocity $\mathbf{v}_i$

$$\mathbf{E}_i = -\int_0^T \mathbf{f}_i(t)\cdot\mathbf{v}_i(t)dt. \tag{1}$$

We adjust the expression of $\mathbf{E}_i$ using impulse $\mathbf{P}_i$ as the independent variable instead of time $T$. $\mathbf{P} \in \mathbb{R}^m$ is the vector of normal impulses. $\mathbf{P}_i$ represents the magnitude of the impulse in contact point $i$, therefore $d\mathbf{P}_i = \mathbf{f}_i dt$. On the other hand, with the Jacobian matrix $\mathbf{J} \in \mathbb{R}^{m\times 6n}$ of contact constraints and the generalized velocity $\dot{\mathbf{q}} \in \mathbb{R}^{6n}$, the relative velocity of contact point $i$ can be represented as $\mathbf{v}_i = \mathbf{J}_i\dot{\mathbf{q}}$. $\mathbf{J}_i$ is the $i$-th row of matrix $\mathbf{J}$. With the new form of $\mathbf{f}_i dt$ and $\mathbf{v}_i$, the potential energy $\mathbf{E}_i$ can be transformed into

$$\mathbf{E}_i = -\int_0^{\mathbf{P}_i} \mathbf{J}_i\dot{\mathbf{q}}d\mathbf{P}_i. \tag{2}$$

In this way we are able to analyze the variation of potential energy while bypassing the dependence on time as a variable. Here $\mathbf{P}_i$ is the normal impulse of point $i$ and it increases during the contact process. The potential energy $\mathbf{E}_i$ will restore to zero at the end of contact. Therefore we seek a set of $P_i$ such that our potential energy is zero once the collision is resolved. Resolving the impulse vector $\mathbf{P}$ that makes all elements in the potential energy vector $\mathbf{E}$ return to zero is the key to the multi-impact system

$$\mathbf{E}(\mathbf{P}) = \mathbf{0}. \tag{3}$$

### 3.1. Quadratic Contact Energy Model

To solve the potential energy equation, we use the *Quadratic Contact Energy* Model. In what follows we derive our model beginning with Eq. 2. The generalized velocity $\dot{\mathbf{q}}$ can be divided into two parts: the initial generalized velocity $\dot{\mathbf{q}}_0$ and the increment caused by the contact impulse $\mathbf{P}$,

$$\dot{\mathbf{q}} = \dot{\mathbf{q}}_0 + \mathbf{M}^{-1}\mathbf{J}^T\mathbf{P}. \tag{4}$$

Then the potential energy at contact point $i$ can be expressed as:

$$\begin{aligned}\mathbf{E}_i &= -\int_0^{\mathbf{P}_i} \mathbf{J}_i\dot{\mathbf{q}}_0 + \mathbf{J}_i\mathbf{M}^{-1}\mathbf{J}^T\mathbf{P}d\mathbf{P}_i \\ &= -(\mathbf{J}_i\dot{\mathbf{q}}_0\mathbf{P}_i + \mathbf{J}_i\mathbf{M}^{-1}\mathbf{J}^T\int_0^{\mathbf{P}_i}\mathbf{P}d\mathbf{P}_i).\end{aligned} \tag{5}$$

In Eq. 5, all variables except $\mathbf{P}$ and $\mathbf{P}_i$ are constant during the contact process. This potential energy will experience a loading-to-unloading cycle and the normal impulse $\mathbf{P}_i$, which makes the energy return to zero. We would like to solve this precisely. In order to compute the integration, the relationship between each element in $\mathbf{P}$ and $\mathbf{P}_i$ is necessary.

Liu et al. [LZB08] started from the force-indentation equation in contact mechanics and discovered a distribution rule for the normal impulses. They found that the ratio of $\frac{d\mathbf{P}_j}{d\mathbf{P}_i}$

can be expressed as the function of $E_{ji}$, which is the ratio of potential energies between contact points $j$ and $i$.

$$\frac{d\mathbf{P}_j}{d\mathbf{P}_i} = \gamma_{ji}^{1/(\eta+1)} (E_{ji}(\mathbf{P}_j, \mathbf{P}_i))^{\eta/(\eta+1)}, \tag{6}$$

where $\gamma_{ji} = k_j/k_i$, $k_j$ and $k_i$ represent the contact stiffness of the $j$-th and $i$-th contact point respectively. $\eta$ indicates the kind of contact ($\eta = 3/2$ for a Hertz contact while $\eta = 1$ in a linear spring model).

With this distribution law, the integration $\int_0^{\mathbf{P}_i} \mathbf{P} d\mathbf{P}_i$ can be performed. Therefore Eq. 5 can be resolved implicitly in the following manner:

$$\mathbf{E}_i(\mathbf{P}_i, \mathbf{E}) = 0. \tag{7}$$

However, resolving this equation directly with Eq. 6 can be time-consuming. This is an implicit equation with a complex expression. Therefore, it cannot be solved easily. In particular, we are interested in an efficient solution. In order to solve Eq. 5 in a reasonable time, we need to find a fast way to compute the relationship between each element in $\mathbf{P}$ and $\mathbf{P}_i$.

There are prior works in mechanics on this ratio, called the *impulse correlation ratio* (ICR) [CH01, AB03], which is generally approximated as a constant. It is described as the ratio of impulse

$$ICR(i) = \frac{\mathbf{P}_i}{\mathbf{P}_{i+1}}. \tag{8}$$

The ICRs depend only on natural modes of the system and the pre-impact velocities [AB03]. ICR makes solving of Eq. 5 easier, as it represents the ratio as a constant. In order to apply ICR to the energy equation, we extend ICR and assume the ratio of $r_{ji} = d\mathbf{P}_j/d\mathbf{P}_i$ is a constant. $r_{ji}$ is the ratio of pre-impact velocities, similar to ICR. That makes the relationship between each element of $\mathbf{P}$ and $\mathbf{P}_i$ obvious. This relationship can be written as a ratio vector $\mathbf{R}^i$, which is defined as:

$$\mathbf{R}^i = \begin{pmatrix} r_{1i} \\ r_{2i} \\ \vdots \\ r_{mi} \end{pmatrix} = \begin{pmatrix} d\mathbf{P}_1/d\mathbf{P}_i \\ d\mathbf{P}_2/d\mathbf{P}_i \\ \vdots \\ d\mathbf{P}_m/d\mathbf{P}_i \end{pmatrix} = \begin{pmatrix} \mathbf{P}_1/\mathbf{P}_i \\ \mathbf{P}_2/\mathbf{P}_i \\ \vdots \\ \mathbf{P}_m/\mathbf{P}_i \end{pmatrix}. \tag{9}$$

The ratio of pre-impact velocities affects the process of impact. Intuitively, a contact point with higher pre-impact velocity will generate higher reaction force, which makes the variation of impulse $d\mathbf{P}_i$ higher than that of other contact points. This phenomena is verified in [KS87]. Therefore, in addition to the theoretical support of ICR, using the ratio of pre-impact velocities to estimate the relationship between each element in $\mathbf{P}$ and $\mathbf{P}_i$ is reasonable.

With vector $\mathbf{R}^i$, $\mathbf{E}_i$ in Eq. 5 can be transformed into a simpler form:

$$\begin{aligned} \mathbf{E}_i &= -(\mathbf{J}_i\dot{\mathbf{q}}_0\mathbf{P}_i + \mathbf{J}_i\mathbf{M}^{-1}\mathbf{J}^T \int_0^{\mathbf{P}_i} \mathbf{P}_i\mathbf{R}^i d\mathbf{P}_i) \\ &= -(\mathbf{J}_i\dot{\mathbf{q}}_0\mathbf{P}_i + \mathbf{J}_i\mathbf{M}^{-1}\mathbf{J}^T\mathbf{R}^i \int_0^{\mathbf{P}_i} \mathbf{P}_i d\mathbf{P}_i) \\ &= -(\mathbf{J}_i\dot{\mathbf{q}}_0\mathbf{P}_i + \frac{1}{2}\mathbf{J}_i\mathbf{M}^{-1}\mathbf{J}^T\mathbf{R}^i\mathbf{P}_i^2). \end{aligned} \tag{10}$$

$\mathbf{R}^i$ is only related with the pre-impact velocity and is constant during the contact process. Therefore it can be pulled out of the integral in Eq. 10. The potential energy of contact point $i$ is now a quadratic function of $\mathbf{P}_i$. Figuring out the $\mathbf{P}_i$ that makes $\mathbf{E}_i$ restore to zero is not expressed as a solution of the differential equation, solving problem any more. Rather it reduces to solving a quadratic equation. It can be solved analytically and is quite cheap. By solving Eq. 10, the contact impulses are acquired and the rigid body dynamics can be resolved.

### 3.2. Multiple Compression

In some complex situations, contact points may experience multiple compression-expansion phases. For example, a contact point may be re-compressed after a contact cycle when it receives the shock wave propagated from other bodies, which is common in the micro process of multi-body collision. It may cause problems for QCE. In Eq. 10, the vector $\mathbf{R}$ is determined by the ratio of pre-impact velocities. Therefore, the corresponding element in $\mathbf{R}$ will be out of date for those contact points that just begin their re-compression phases. This is because the corresponding ratio is calculated with the velocity in the previous compression cycle. However, the pre-impact velocity in the current compression cycle should be zero at the beginning of its re-compression. Therefore the new velocity ratio, either zero or infinite, is not correct.

To overcome this problem, we use an iterative solution to separate multiple compression-expansion phases. In each iteration, a contact point can only experience one compression-expansion phase. If the relative velocity of this point becomes negative once again, the violation should be temporarily ignored and be delayed to the next iteration. This means that the problem caused by zero velocity at the beginning of the re-compression phase can be avoided. The iterations will be terminated when no more violations exist and the total impulses can be computed by simply adding the results from each iteration together. Let $\lambda_c \in \mathbb{R}^m$ denote the total impulse and $\lambda^s \in \mathbb{R}^m$ denote the result from the $s$-th iteration,

$$\lambda_c = \sum_{s=1}^{num} \lambda^s \tag{11}$$

where *num* is the iteration count.

If a contact point, e.g. the $j$-th point, still has potential energy, it will keep applying force to each body. After an

expansion phase, the potential energy will restore to zero and no force will persist at this point. The vanishing of such force has influence on neighbor contact points because if $d\mathbf{P}_j$ drops to zero, the $j$-th element of $\mathbf{R}^i$ should change from a non-zero constant $r_{ji}$ to zero (Eq. 9). Therefore, after solving the impulse $\mathbf{P}_j$ of contact point $j$, all the points belonging to the same bodies as $j$ should reconstruct their energy equations.

Fig. 3 shows the flowchart that QCE works, corresponding to the pseudo code in Alg. 1. A QCE step consists of multiple iterations which represent multiple compression. The termination check module, which will return true only if no violation is detected, determines whether to terminate the iteration or not. During each iteration, all of the energy equations are initialized. Three steps, shown in the dotted lines, are repeated until the solution list is empty. This can resolve the multiple compression-expansion process. Within each loop, the minimal solution is selected first and the corresponding impulse is recorded. Then the energy equations of neighbor contact points are updated and the solutions are recalculated as discussed above. After all solutions are selected, the loop in the dotted lines will be terminated within one simulation time step. Finally, the impulses are applied in order to update the generalized velocity. This process is repeated until no violations are detected.

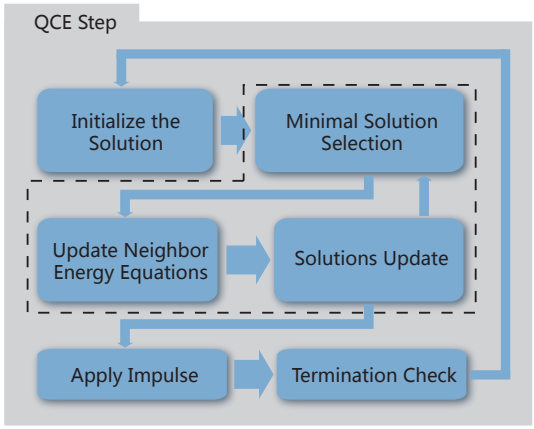


**Figure 3:** *Flowchart of the QCE steps.*

### 3.3. Solver of Quadratic Contact Energy Model

According to Eq. 10, which describes the potential energy of every contact point, we rewrite Eq. 3 as:

$$\mathbf{E}(\mathbf{P}) = \mathbf{A} \circ \mathbf{P} \circ \mathbf{P} + \mathbf{B} \circ \mathbf{P} + \mathbf{C} = \mathbf{0}. \tag{12}$$

Vectors $\mathbf{A}$, $\mathbf{B}$ and $\mathbf{C}$ correspond to the coefficients of quadratic equations. $\circ$ is the Hadamard product (also known as the entrywise product), which multiplies corresponding elements of two matrices or two vectors with the same dimension. Computing $\mathbf{A}$, $\mathbf{B}$ and $\mathbf{C}$ from Eq. 10 directly can be difficult. According to Eq. 9, the vector $\mathbf{R}^i$ is different for each contact point. Notice that because the pre-impact velocity of a given contact point $i$ has the possibility of being zero, this may result in a exceptional value to the ratio $r_{ji}$ when the denominator term corresponds to zero pre-impact velocity. In order to solve this problem, we use the vector $\mathbf{F}$ instead of $\mathbf{R}^i$ for all the contact points. $\mathbf{F}$ is the vector of pre-impact velocities and the $j$-th element of $\mathbf{R}^i$ is $\mathbf{F}_j/\mathbf{F}_i$, $\mathbf{F} = \mathbf{F}_i\mathbf{R}^i$ for any contact point $i$. We then multiply $\mathbf{F}_i$, which is non-zero, to both sides of Eq. 9,

$$\mathbf{F}_i\mathbf{E}_i = \mathbf{J}_i\dot{\mathbf{q}}_0\mathbf{F}_i\mathbf{P}_i + 1/2\mathbf{J}_i\mathbf{M}^{-1}\mathbf{J}^T\mathbf{F}\mathbf{P}_i^2. \tag{13}$$

This multiplication does not change the result. However, it enables $\mathbf{A}$, $\mathbf{B}$ and $\mathbf{C}$ to be expressed in a simpler way as

$$\mathbf{F}_i\mathbf{E}_i = \mathbf{A}_i\mathbf{P}_i^2 + \mathbf{B}_i\mathbf{P}_i + \mathbf{C}_i. \tag{14}$$

The initial values of $\mathbf{A}$, $\mathbf{B}$ and $\mathbf{C}$ can be expressed as:

$$\begin{aligned} \mathbf{A} &= 1/2\mathbf{J}\mathbf{M}^{-1}\mathbf{J}^T\mathbf{F} \\ \mathbf{B} &= \mathbf{F} \circ \mathbf{J}\dot{\mathbf{q}}_0 \\ \mathbf{C} &= \mathbf{0}, \end{aligned} \tag{15}$$

and the energy equation becomes

$$\mathbf{F} \circ \mathbf{E}(\mathbf{P}) = \mathbf{0}. \tag{16}$$

During the multi-contact process, interactions between different contact points start concurrently but may terminate individually. As discussed in Section 3.2, once a point ends its contact, the energy equations of all neighbor contact points need to be recomputed. Therefore, the sequence of contact terminations is important for the final result. As the time variable is eliminated in Eq. 2, we have to search for a substitute to compute the sequence of terminations. For any contact point $i$ with non-zero pre-impact velocity, let $\mathbf{P} = \mathbf{P}_i\mathbf{R}^i$ according to Eq. 9 and $\mathbf{F}_i\mathbf{R}^i = \mathbf{F}$, therefore,

$$\mathbf{P} = (\mathbf{P}_i/\mathbf{F}_i)\mathbf{F}, \tag{17}$$

where $\mathbf{F}_i$ is fixed and $\mathbf{P}_i$ increases during the contact. This steadily increasing variable $\mathbf{P}_i/\mathbf{F}_i$ is the 'time-like' independent variable that we want and we use variable $s$ to express it as:

$$\mathbf{P} = s\mathbf{F}. \tag{18}$$

For any contact point $k$, it has a corresponding impulse $\mathbf{P}_k$ making its potential energy return to zero. There exists a certain $s_k$ corresponding to the time of termination. The smaller $s_k$ is, the earlier the contact process is finished. All the $s_k$'s can be computed by solving Eq. 14 at the beginning. The algorithm repeatedly selects the smallest from them, then terminates its impact process, and recomputes the energy equations of neighboring contact points. The reconstruction is shown in Alg. 1, on line 20 - 26. Notice that the quadratic equation in our algorithm has two roots $r_1$ and $r_2$, $r_1 \leq s_k \leq r_2$. Only the larger root $r_2$ is chosen because $s$ which represents the contact process never decreases.

According to Alg. 1, selecting the smallest element from a $m$-dimension vector $\mathbf{S}$ has complexity of $O(m)$(line 14). However, this is expensive as this step is performed $m$ times during each iteration. To speedup the algorithm, we use a min-heap, instead of a vector, as the underlying data structure for $S$. Building a min-heap has the complexity $O(mlog(m))$, while popping the smallest element from the heap takes $O(log(m))$ time, including $O(1)$ for getting the element from the top of heap and $O(log(m))$ for filtering down. The average number of neighboring contact points within the same object can be considered as a constant and has no relationship with $m$; therefore, the reconstruction of equations after the selection takes $O(1)$ time. The most time-consuming step during each iteration is the construction of min-heap, which takes $O(mlog(m))$. Overall, the complexity of one iteration is $O(mlog(m))$.

**Algorithm 1** Quadratic Contact Energy

```
1:  procedure QUADRATICCONTACTENERGY(q, q̇)
2:      q̇_c ← q̇
3:      while true do
4:          //Solutions Initialization
5:          F ← max(−Jq̇_c, 0)
6:          A ← 1/2 JM^{-1}J^T F
7:          B ← F ∘ Jq̇_c
8:          C ← 0, S ← 0, P ← 0
9:          for all contact points, k do
10:             S_k ← SolveQuadratic(A_k, B_k, C_k)
11:         end for
12:         while S is not all-zero do
13:             //Minimal Solution Selection
14:             find the smallest non-zero element S_k in S
15:             P_k ← F_k * S_k
16:             S_k ← 0
17:             for all contact points, i do
18:                 if (JM^{-1}J^T)_ik ≠ 0 and P_i = 0 then
19:                     //Neighbor Equation Update
20:                     curP ← F_i S_i
21:                     curE ← A_i curP^2 + B_i curP + C_i
22:                     A_i ← A_i + (JM^{-1}J^T)_ik J_k
23:                     B_i ← B_i − (JM^{-1}J^T)_ik J_k P_k
24:                     C_i ← curE − (A_i curP^2 + B_i curP)
25:                     //Solutions Update
26:                     S_i ← SolveQuadratic(A_i, B_i, C_i)
27:                 end if
28:             end for
29:         end while
30:         //Apply Impulse
31:         q̇_c ← q̇_c + M^{-1}J^T P
32:         //Termination Check
33:         if No element in q̇_c is less than zero then
34:             return q̇_c
35:         end if
36:     end while
37: end procedure
```

## 4. Restitution and Friction

Restitution is modeled from the change of potential energy with Stronge's hypothesis in [Mir96]. Since analyzing the potential energy for each contact point in QCE is quite intuitive and effective, it is fine to couple Stronge's hypothesis with QCE to simulate restitution. However, simple combinations may result in inelastic collapse. With an iterative strategy similar to GR, the count of iteration increases rapidly when the coefficient of restitution becomes small. This makes it difficult to model the restitution directly by potential energy.

Fortunately, our QCE model can also be embedded into LCP to simulate a scenario with restitution and friction. Generally, resolving the LCP requires the prediction of post-impact velocity. The negative value of pre-impact velocity $\dot{\mathbf{q}}_0$ is adopted in LCP. This inaccurate prediction is the main reason for LCP's violation in (BRK) [SKV*12]. QCE can overcome this problem because the reliable post-impact velocity $\dot{\mathbf{q}}_c^+ \in \mathbb{R}^{6n}$ is available. $\dot{\mathbf{q}}_c^+$ can be used as the prediction of post-impact velocity instead of $-\dot{\mathbf{q}}_0$. Therefore, the QCE-LCP equation has the form of

$$\mathbf{0} \leq \lambda \perp \mathbf{J}\mathbf{M}^{-1}\mathbf{J}^T\lambda + \mathbf{J}\dot{\mathbf{q}}_0 \geq c_r\mathbf{J}\dot{\mathbf{q}}_c^+, \tag{19}$$

where $\lambda \in \mathbb{R}^m$ is the vector of normal impulses' magnitudes and $c_r$ represents the coefficient of restitution. QCE-LCP degenerates to standard LCP when $c_r = 0$, i.e. it generates the same result as standard LCP in purely in-elastic multi-impact cases. QCE-LCP will generate the same result as QCE when $c_r = 1$. Otherwise, in the case of $0 < c_r < 1$, QCE-LCP is a mix of standard LCP and QCE. In this way, the restitution problem can be nicely solved.

In order to resolve friction, boxed LCP (BLCP) [TBV12, ST96] can be used. A boxed LCP, $\mathbf{x} = \mathbf{BLCP}(\mathbf{A}, \mathbf{b}, \mathbf{l}, \mathbf{h})$, is defined as

$$\begin{aligned} &\text{find } \mathbf{x} \in \mathbb{R}^m \text{such that, for all } i = 1..m, \\ &\quad \mathbf{x}_i = \mathbf{l}_i \text{ and } (\mathbf{A}\mathbf{x}+\mathbf{b})_i \geq 0 \text{ or} \\ &\quad \mathbf{x}_i = \mathbf{h}_i \text{ and } (\mathbf{A}\mathbf{x}+\mathbf{b})_i \leq 0 \text{ or} \\ &\quad \mathbf{l}_i < \mathbf{x}_i < \mathbf{h}_i \text{ and } (\mathbf{A}\mathbf{x}+\mathbf{b})_i = 0. \end{aligned} \tag{20}$$

The coupling of normal contact impulses $\lambda$ and friction impulses $\lambda_f$ can be expressed by the following formulation:

$$\begin{aligned} \lambda &= \mathbf{QCE\text{-}LCP}(\mathbf{J}\mathbf{M}^{-1}\mathbf{J}^T, \mathbf{J}\dot{\mathbf{q}}_0 + \mathbf{J}\mathbf{M}^{-1}\mathbf{D}^T\lambda_f) \\ \lambda_f &= \mathbf{BLCP}(\mathbf{D}\mathbf{M}^{-1}\mathbf{D}^T, \mathbf{D}\dot{\mathbf{q}}_0 + \mathbf{D}\mathbf{M}^{-1}\mathbf{J}^T\lambda, \\ &\qquad -\mathbf{diag}(\mu)\lambda, \mathbf{diag}(\mu)\lambda). \end{aligned} \tag{21}$$

**D** is the Jacobian matrix of the discretized friction pyramid. This set of equations can not be solved directly. Rather, we can run one PGS iteration on the first equation, followed by another PGS iteration on the second and then repeat the process. In this way, we can get the result in just a few iterations. The restitution and friction parts of QCE-LCP won't break the physical desiderata like (SYM) or (KIN) since LCP and BLCP always keep the symmetry preserved and the energy bounded.

## 5. Results and Analysis

First we will exhibit the three-ball chain scenario. This scenario demonstrates the ability of QCE to simulate the wave effect. We then use identical objects to show the accuracy of QCE. In order to test the application range of our model, we simulate granular objects and some complex scenarios. The results are robust and reliable. All the simulations are performed on a PC with 3.00GHz Intel i5 CPU, 4G RAM.

| MODEL | WAV | BRK | SYM | KIN | MON | ONE |
|---|---|---|---|---|---|---|
| ***QCE*** | • | • | • | • | • | • |
| GR | × | • | • | • | • | • |
| LCP | × | × | • | • | • | • |

**Table 1:** *Multi-impact feature chart. Our model satisfies all the six physical desiderata while previous models fail in one or more of them.*

### 5.1. Three-ball Chain

Three-ball chain is an ideal scenario to examine (WAV). A typical three-ball chain is shown in Fig. 2. At the beginning, the ball $B$ rests in the middle while the other balls, $A$ and $C$, have different approaching velocities. According to [Pay08], $A$ and $C$ should change their velocities while $B$ remains still.

To quantitatively analyze the post-impact velocities, we set $C$'s velocity to a constant $v_0$ while $A$'s velocity is given by the independent variable $v_a^-$. Then the post-impact velocities $v_a^+$, $v_b^+$ and $v_c^+$ are all determined by the value $v_a^-$. All velocities are normalized by $v_0$ as shown in Fig. 4.

When $v_a^- = 0$, QCE matches the theoretical expectation. With this value of $v_a^-$, the test case is *Newton's Cradle*, in which LCP fails to satisfy (BRK). Smith et al. [SKV*12] solve this problem by introducing GR, making the result correct at $v_a^- = 0$. However, there is no difference between GR and LCP when $v_a^-$ doesn't equal zero. When two contact points both have negative relative velocities, the violator subset used in GR is the same as the active set in LCP. As a result, GR and LCP generate the same results. In Fig. 4, it means GR's curves totally match LCP's except at $v_a^- = 0$. For this reason, GR's results are not rendered individually.

When $v_a^- = v_0$, both QCE and LCP generate the correct result. This is caused by the constraint of symmetry preservation. When $A$ and $C$ have the same approaching velocity, the test case is symmetric and should remain symmetric after collision. Clearly, both models satisfy (SYM).

As for other values of $v_a^-$, there is no correlation between LCP's outcome and the theoretical expectation. This is caused by the inaccurate prediction of post-impact velocity [SKV*12]. In contrast, our model is closer to the expectation. This is obvious when observing the velocities of post-impact $v_a^+$, $v_b^+$ and $v_c^+$ of the balls in Fig. 4. Since the ICR used in QCE is an approximation for wave propagation, QCE doesn't completely match the ideal curve as a result. Actually, if we use Eq. 6, without the ICR approximation, the equation used to represent the potential energy will be precise enough to obtain the exact answers. It is a trade-off between precision and time complexity. In any case, the velocity curve of QCE matches the theoretical formulation for all values and demonstrates that QCE is more accurate than both GR and LCP.

### 5.2. Identical Objects

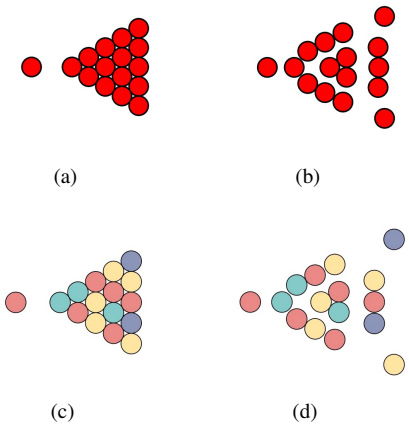


**Figure 5:** *Pool Break of billiards. A rack of billiard balls is hit by a moving one. The results of (b) QCE and (d) GR are highly similar to each other. Both models generate clean pool breaks with symmetric patterns. (c) and (d) are extracted from the video of [Smith et al. 2012]*

Given their simplicity, identical spheres are ideal simulation objects to test the accuracy of a contact model. The theoretical result of a collision can be easily computed.

We first use the *Pool Break* scenario to exhibit the clean and symmetric pattern. A billiard ball is fired along the axis of symmetry towards a rack of 15 billiard balls at rest. The billiard balls are initially symmetric, thus requiring the symmetry to be strictly preserved after impact. At the instant of contact, the shock wave propagates in the rack of billiard

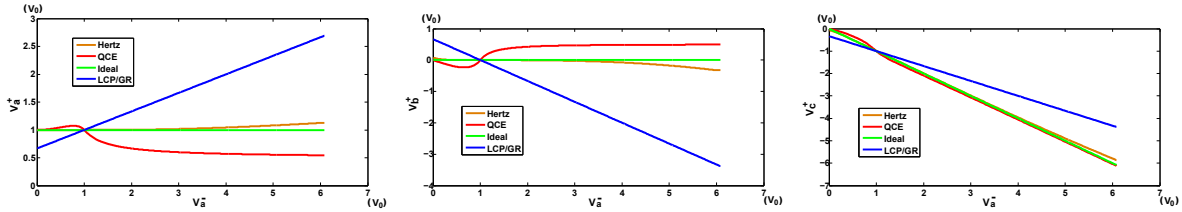


**Figure 4:** *The accuracy comparisons when simulating the case corresponding to Fig. 2 using different models. We set the pre-impact velocity of C to be constant $v_0(v_c^- = v_0)$, $v_b^- = 0$, while the velocity of A is the independent variable $v_a^-$. The ordinate axis represents the post-impact velocity of ball A($v_a^+$), B($v_b^+$) and C($v_c^+$) respectively. The unit of velocity is m/s.*

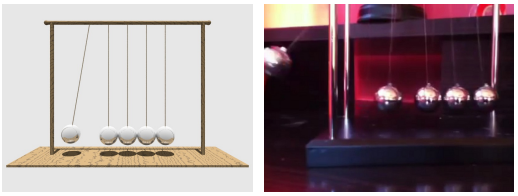


**Figure 6:** *3D Newton's Cradle. (a) Stationary balls in a line are hit by other moving balls; (b) the phenomenon of breaking away is generated.*

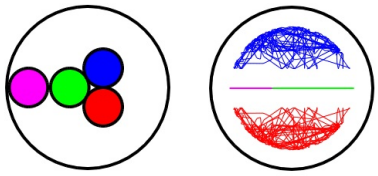


**Figure 7:** *Symmetry preservation test. (a) Four balls are placed in a circle. (b) After long-term simulation, the trajectories of balls are still symmetric.*

balls from left to right. GR is the first model capable of simulating the breaking-away effect while preserving the symmetry. The pattern of billiard balls after impact is clean and symmetric. This pattern could not be achieved by either LCP or pair-wise approaches like Gauss-Siedel or Jacobi. We apply QCE to the *Pool Break* and successfully get a nice pattern. We compare the results of QCE and GR in Fig. 5 and find high similarity between them. As with GR, our model generates clean pool breaks with symmetric patterns.

*Newton's Cradle* is another ideal scenario to demonstrate the importance of (WAV). It would not be possible to simulate many phenomena without accounting for wave propagation. Initially contacting spheres cannot break away during simulation. In fact, shock waves together with momentum and energy propagate in the spheres at the instant of impact. This micro-process, which is ignored by current models, is the base of our model. As a result, the simulation result of our model for *Newton's Cradle* is highly comparable to reality.

In order to validate QCE's capability of (SYM), we duplicate the four-ball experiment in [SKV*12]. As shown in Fig. 7, four balls are placed in a circle and the initial velocities are symmetric. In this example QCE preserves symmetry well during the long-term simulation. This can be easily observed from the trajectory of balls in Fig. 7.b.

### 5.3. Granular Objects

| Pattern | Iteration | | | Time cost | | |
|---|---|---|---|---|---|---|
| | avg | max | min | avg | max | min |
| Square | 13 | 46 | 1 | 0.28 | 2.74 | 0.00 |
| Strip | 17 | 44 | 1 | 0.33 | 4.39 | 0.00 |
| Hex | 12 | 33 | 1 | 0.25 | 2.87 | 0.00 |

**Table 2:** *Convergence and performance statistics for extended patterns. We report the max, min and average number of iteration for the QCE step. We also report the total time (in seconds) spent in contact resolving (including QCE and BLCP step). All the examples are simulated with a fixed timestep of 0.0002s. Timings are recorded with a single thread on a 3.00GHz Intel Core i5-2320.*

Wave propagation is commonly observed in granular simulation. The experiment in [JNB96] shows a nice wave pattern of granular objects after a single shock. Therefore we duplicate this experiment wherein 4,000 granules fall into a container. After the pile comes to rest, each granule is colored by its depth as displayed in Fig. 8.a. These horizontal stripes are composed of grains with the same depth and function as labels of layers. Then a single vertical shake of the

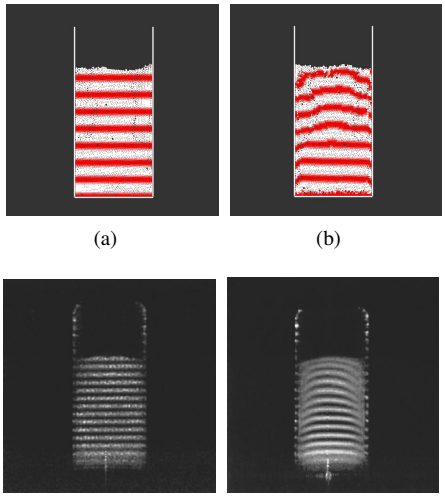

(a) (b) (c) (d)

**Figure 8:** *Shock wave pattern. (a) Stationary granular objects in a container are labeled by their depths. (b) After a single shake, the pattern of wave propagation can be clearly observed. We compare the pattern (c) to the experiment result (d) from [Jaeger et al. 1996] and find high similarity between them.* $c_r = 0.3$ *and* $\mu = 0.2$ *in this experiment.*

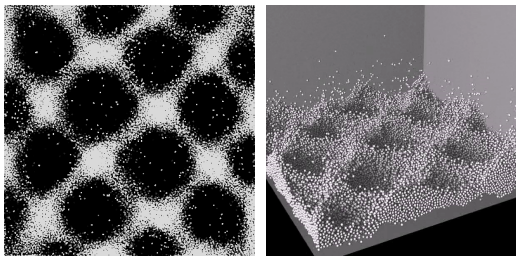

(a) (b)

**Figure 9:** *The extended patterns. (a) The height map of vibrating granules. (b) After rendering the pattern is very clear. All parameter settings are the same with [BSS*98].*

container is carried out and shock waves propagate from bottom to top. In Fig. 8.b the pattern of wave can be clearly observed. This pattern matches well with the experiment result of [JNB96] in Fig. 8.d. Therefore the ability of QCE to satisfy (WAV) is further proved. Through generating the same wave pattern with experimental results, we demonstrate that our model is reliable.

As mentioned in [SKV*12], the extended patterns of massive granules on a vibrating floor are ideal computational benchmarks to examine both *validation* and *efficiency*. In order to generate the extended patterns, accurate resolution of multi-impacts with high velocity is required. The scaling and performance are also examined in such a large scene. In order to validate our model and examine the performance, we duplicate the experiment of extended patterns in [BSS*98] where 60,000 granules fall on a vibrating floor. With different amplitudes and frequencies, three patterns are generated and correspond to the experimental results in [BSS*98]: squares at $(f^* = 0.27, \Gamma = 3.00)$, stripes at $(f^* = 0.44, \Gamma = 3.00)$ and hexagons at $(f^* = 0.38, \Gamma = 4.00)$. This experiment further proves that the results from our model are plausible.

The convergence and performance statistics of extended patterns are reported in Table 2. The iteration step in QCE converges in all the examples. Benefitting from the quadratic form of contact energy, our model improves the performance significantly while maintaining the accuracy. The average time cost for frictional contact resolution in Hex is 0.25s. With the same parameters, GR spends 6.1s on an average according to [SKV*12].

### 5.4. Complex Scenarios

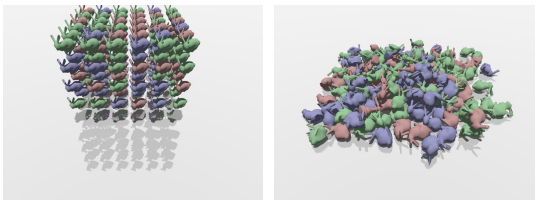

(a) (b)

**Figure 10:** *(a) Bunnies fall onto the ground and are hit by falling pawns. (b) After energy dissipation during the collapse, these bunnies and pawns rest on the floor in a pile.* $c_r = 0.2$ *and* $\mu = 0.2$ *in this experiment.*

So far, the experiments designed above are frictionless for simplicity. In fact, friction is significant in rigid body simulation. To examine the behavior of QCE-LCP under frictional conditions, we build a *Card House* composed of 24 thin plates. Card house is a delicate structure, which is stable only with precise resolution of normal impulses, tangential impulses and their coupling. We find that by using our model, the card house remains still, indicating the high accuracy of contact impulse resolving. Moreover, after being hit with two balls, the card house collapses and these thin plates collide with each other during the course of collapse. At last, all the plates rest on the floor in a pile with all kinetic energy dissipated by friction. Both static friction and dynamic friction are well simulated in the accompanying video.

In order to examine the generality, we design a more complex case called Rube Goldberg machine. It includes several typical parts mentioned above, e.g., *Newton's Cradle*, *Card House*, and *Pool Break*. Tracks are used as the chains to link each part of the Rube Goldberg machine. Notice that this

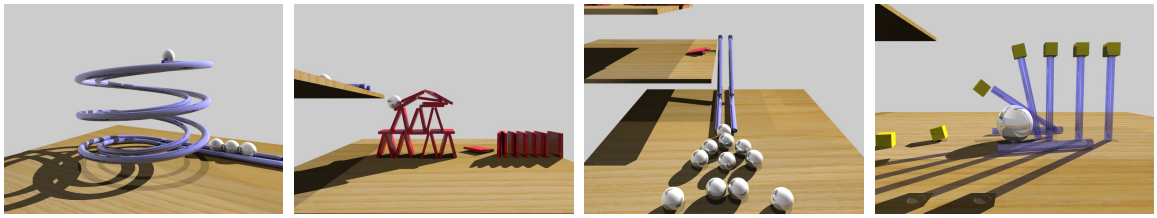

(a) (b) (c) (d)

**Figure 11:** *The Rube Goldberg machine composed of Newton's Cradle, Card House and Pool Break.*

scenario is simulated as a whole rather than joining several individual parts together. The whole process is well-designed and even a small error can break the chain of reactions. A rigid ball first rolls down a spiral track and hits three other balls resting on a straight track. As in *Newton's Cradle*, the last one of the three balls flies out of the track and hits a card house, causing it to collapse. One piece of thin plate hits the domino when falling down causing the dominos to fall one by one. The last domino falls off of the table and drops on one side of a seesaw. On the other side, a resting ball is triggered by the seesaw and drops on an oblique track, speeding up towards a rack of ten billiard balls. After a clean pool break, one billiard ball in the corner drops on another spiral track, rolls down and finally knocks down several pillars in a row. Our model successfully simulates this Rube Goldberg machine with all parts working as expected. The whole process can be seen in the video.

Our method has high robustness for not only identical objects, but also for models represented using complex meshes. To demonstrate this, we simulate 144 bunnies falling onto the ground and then being hit by 16 pawns. The figure and accompanying video show that our approach behaves well during these tests and no crash or exception appears.

According to section 3.1, QCE is based on the variation of contact energy. Therefore, QCE should be capable of preserving the kinetic energy, satisfying (KIN). In order to examine this, we analyze the total kinetic energy before and after the QCE step. Given the pre-QCE energy $E^-$ and post-QCE energy $E^+$, we use $e$ to measure the error ratio, where $e = |E^- - E^+|/E^-$. In the scenario of falling bunnies and pawns, the average $e$ is 0.000243. This proves that QCE can preserve the kinetic energy well. Therefore, (KIN) can be satisfied.

### 5.5. Robustness

Numeric error and its accumulation may occur during the simulation. The robustness of simulation can be examined by these problems. For example, in the *Newton's Cradle* the relative velocity of the contact points are generally considered as zero. However, in most cases the relative velocities are not strictly equal to zero due to the numeric error accumulation after long time steps. As shown in Fig. 12, we examine the robustness of QCE and GR using the *Newton's Cradle* with disturbance to simulate the numeric error. All the balls are initially in contact. The ball on the leftmost has an initial velocity while others are still. At the instant of impact, we add random disturbance to the relative velocities of all contact points. The value of disturbance is much less than the impact velocity.

In theory, this disturbance should have little effect on the result. It should obey the rule that as the disturbance becomes infinitely small, its influence would also become infinitely small. It can be easily verified with the Hertz contact model. In Fig. 4, when $v_a^-$ is close to zero, the pre-impact velocity between ball A and B can be considered as the disturbance. It's obvious that both the ideal result and the Hertz model show continuity of results. They are hardly influenced by the disturbance. GR is very sensitive and shows discontinuity in its results. It generates many results with varying disturbance, but none of them confirms the expected break-away effect. On the contrary, QCE demonstrates improved robustness and is more accurate than GR. It can simulate break-away effects, irrespective of whatever disturbance is added. QCE is based on the potential energy analysis of each contact point, therefore the added disturbance has no influence on the results for QCE.

## 6. Limitations and Future Work

We propose a novel contact model for multi-impact simulation. Inspired by engineering mechanics, we model the potential energy of each contact point and analyze its change during the contact process. The quadratic contact energy model, which can be resolved analytically without numerical error, generates feasible results that satisfy all the six physical desiderata, including WAV. By embedding the quadratic contact energy model with standard LCP, we propose QCE-LCP, which is able to simulate the effect of restitution and friction. QCE-LCP inherits advantages from both models and we have highlighted its performance for many complex scenarios.

In order to model restitution and friction, we combine QCE with LCP. This is because using the Stronge's Hypoth-

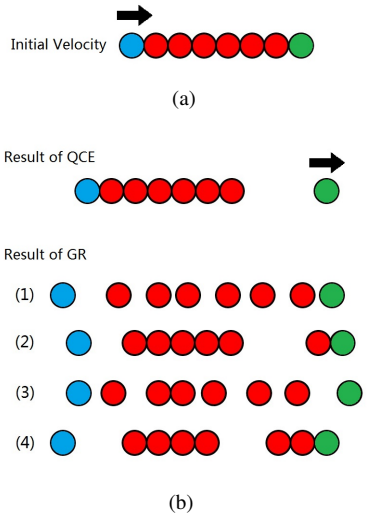


**Figure 12:** *(a) The* Newton's Cradle *with random disturbance in order to examine the robustness. (b) Comparison between the results of QCE and GR. GR generates different results with different disturbance.*

esis, similar to [Mir96], causes inelastic collapse. This is not a useful computation because the varying process of potential energy has already been analyzed in QCE. If the problem of inelastic collapse can be solved, restitution can be modeled more precisely. Intuitively the effect caused by different materials of objects can also be modeled through potential energy. This is a good topic for future work.

In our model we use an iterative strategy. While our approach matches the results with real-world behaviors and simulations, we don't have a rigorous proof related to its termination. The iteration converges for all examples that we have tested so far. But it's hard to prove the convergence mathematically. Moreover, if we can provide rigorous guarantees on its termination and convergence, that can also be used to improve the iteration count and accelerate the computation.

For a single iteration, the computational complexity is $O(mlog(m))$, where $m$ is the number of contact points. This makes QCE slower than LCP with a PGS solver. We don't know whether $O(mlog(m))$ is the lower bound for our model. The main reason that this results in such complexity is the repeated computation and selection of the smallest value in a vector using the min-heap. If this selection can be somehow be skipped or replaced by a faster operation, it can accelerate our computation. Finally, we would like to further evaluate its performance on complex real-world simulation scenarios.

## Acknowledgement

We would like to thank the anonymous reviewers for the invaluable comments. This research was supported by Grant Nos. 61170205, 61232014, 61421062, 61472010 from National Natural Science Foundation of China. It was also jointly supported by the research grant from Beida (Binhai) Information Research. Hanqiu Sun was partially supported by RGC research grant (ref. 416212).

## References

[AB03] ACARY V., BROGLIATO B.: Concurrent multiple impacts modelling: Case-study of a 3-ball chain. In *Computational Fluid and Solid Mechanics. Second Mit Conference 2003* (cambridge, États-Unis, 2003), Bathe K., (Ed.), MIT, Elsevier. 4

[AP97] ANITESCU M., POTRA F. A.: Formulating dynamic multi-rigid-body contact problems with friction as solvable linear complementarity problems. *Nonlinear Dynamics 14* (1997), 231–247. 2, 3

[Bar89] BARAFF D.: Analytical methods for dynamic simulation of non-penetrating rigid bodies. *SIGGRAPH Comput. Graph. 23*, 3 (July 1989), 223–232. 2

[Bar91] BARAFF D.: Coping with friction for non-penetrating rigid body simulation. *SIGGRAPH Comput. Graph. 25*, 4 (July 1991), 31–41. 2

[BET14] BENDER J., ERLEBEN K., TRINKLE J.: Interactive simulation of rigid body dynamics in computer graphics. *Computer Graphics Forum 33*, 1 (2014), 246–270. 2

[Bro99] BROGLIATO B.: *NONSMOOTH MECHANICS.: Models, Dynamics and Control, Second edition*. Communications and Control Engineering. Springer London, 1999. 2

[BSS*98] BIZON C., SHATTUCK M., SWIFT J., MCCORMICK W., SWINNEY H. L.: Patterns in 3d vertically oscillated granular layers: simulation and experiment. *Physical review letters 80*, 1 (1998), 57. 9

[CH01] CEANG V., HURMUZLU Y.: A new look at an old problem: Newton cradle. *Journal of Applied Mechanics, Transactions of A.S.M.E 68* (2001), 575–583. 4

[CR98] CHATTERJEE A., RUINA A.: A new algebraic rigid-body collision law based on impulse space considerations. *Journal of Applied Mechanics 65* (1998), 939–951. 2

[Erl04] ERLEBEN K.: Stable, robust, and versatile multibody dynamics animation. *Ph. D. Thesis, University of Copenhagen, Copenhagen* (2004). 2

[Erl07] ERLEBEN K.: Velocity-based shock propagation for multibody dynamics animation. *ACM Trans. Graph. 26*, 2 (June 2007). 3

[GBF03] GUENDELMAN E., BRIDSON R., FEDKIW R.: Nonconvex rigid bodies with stacking. *ACM Trans. Graph* (2003), 871–878. 3

[Hah88] HAHN J. K.: Realistic animation of rigid bodies. *SIGGRAPH Comput. Graph. 22*, 4 (June 1988), 299–308. 2

[HHL99] HASCOËT E., HERRMANN H. J., LORETO V.: Shock propagation in a granular chain. *Phys. Rev. E 59* (Mar 1999), 3202–3206. 3

[JMSS07] JOB S., MELO F., SOKOLOW A., SEN S.: Solitary wave trains in granular chains: experiments, theory and simulations. *Granular Matter 10*, 1 (2007), 13–20. 3

[JNB96] JAEGER H. M., NAGEL S. R., BEHRINGER R. P.: Granular solids, liquids, and gases. *Reviews of Modern Physics 68*, 4 (1996), 1259–1273. 8, 9

[KS87] KHULIEF Y., SHABANA A.: A continuous force model for the impact analysis of flexible multibody systems. *Mechanism and Machine Theory 22*, 3 (1987), 213 – 224. 3, 4

[LN90] LANKARANI H., NIKRAVESH P.: A contact force model with hysteresis damping for impact analysis of multibody systems. *Journal of Mechanical Design 112* (1990), 369. 3

[LN94] LANKARANI H., NIKRAVESH P.: Continuous contact force models for impact analysis in multibody systems. *Nonlinear Dynamics 5*, 2 (1994), 193–207. 3

[LZB08] LIU C., ZHAO Z., BROGLIATO B.: Frictionless multiple impacts in multibody systems. i. theoretical framework. *Proceedings of the Royal Society A: Mathematical, Physical and Engineering Science 464*, 2100 (2008), 3193–3211. 3

[MC95] MIRTICH B., CANNY J.: Impulse-based simulation of rigid bodies. In *Proceedings of the 1995 symposium on Interactive 3D graphics* (1995), ACM, pp. 181–ff. 2

[Mir96] MIRTICH B. V.: *Impulse-based Dynamic Simulation of Rigid Body Systems*. Tech. rep., 1996. 6, 11

[Mur88] MURTY K.: *Linear complementarity, linear and nonlinear programming*. Sigma series in applied mathematics. Heldermann, 1988. 2

[NB14] NGUYEN N. S., BROGLIATO B.: *Multiple impacts in dissipative granular chains*. Springer, 2014. 3

[NE15] NIEBE S., ERLEBEN K.: *Numerical Methods for Linear Complementarity Problems in Physics-Based Animation*. Morgan & Claypool Publishers, 2015. 2

[Pay08] PAYR M. D.: *An experimental and theoretical study of perfect multiple contact collisions in linear chains of bodies*. PhD thesis, ETH, 2008. 2, 7

[PPG04] PAULY M., PAI D. K., GUIBAS L. J.: Quasi-rigid objects in contact. In *Proceedings of the 2004 ACM SIGGRAPH/Eurographics symposium on Computer animation* (2004), Eurographics Association, pp. 109–119. 3

[SH96] STOIANOVICI D., HURMUZLU Y.: A critical study of the applicability of rigid-body collision theory. *Journal of Applied Mechanics 63* (1996), 307–316. 3

[SHB*08] SEN S., HONG J., BANG J., AVALOS E., DONEY R.: Solitary waves in the granular chain. *Physics Reports 462*, 2 (2008), 21–66. 2

[SKV*12] SMITH B., KAUFMAN D. M., VOUGA E., TAMSTORF R., GRINSPUN E.: Reflections on simultaneous impact. *ACM Trans. Graph. 31*, 4 (July 2012), 106:1–106:12. 2, 6, 7, 8, 9

[SM01] SEN S., MANCIU M.: Solitary wave dynamics in generalized hertz chains: An improved solution of the equation of motion. *Phys. Rev. E 64* (Oct 2001), 056605. 3

[ST96] STEWART D., TRINKLE J. C.: An implicit time-stepping scheme for rigid body dynamics with coulomb friction. *International Journal for Numerical Methods in Engineering 39* (1996), 2673–2691. 6

[Ste00] STEWART D.: Rigid-body dynamics with friction and impact. *SIAM Review 42*, 1 (2000), 3–39. 2

[TBV12] TONGE R., BENEVOLENSKI F., VOROSHILOV A.: Mass splitting for jitter-free parallel rigid body simulation. *ACM Trans. Graph. 31*, 4 (July 2012), 105:1–105:8. 2, 6

[WLN*13] WILLIAMS J., LU Y., NIEBE S., ANDERSEN M., ERLEBEN K., TRINKLE J. C.: Rpi-matlab-simulator: A tool for efficient research and practical teaching in multibody dynamics. In *VRIPHYS* (2013), pp. 71–80. 2

## Appendix

**Lemma.** $\lambda_c$ is a feasible solution to the QCE-LCP equation in purely elastic collision.

*Proof* $\lambda_c$ is the sum of $\lambda^s$ according to Eq. 11 and each element in $\lambda^s$ is no less than zero, thus $\mathbf{0} \le \lambda_c$. After the impulse $\lambda_c$ is adopted, the post-impact velocity is represented as $\mathbf{M}^{-1}\mathbf{J}^T\lambda_c + \dot{\mathbf{q}}_0$, which is actually $\dot{\mathbf{q}}_c^+$ as the following:

$$\mathbf{J}\mathbf{M}^{-1}\mathbf{J}^T\lambda_c + \mathbf{J}\dot{\mathbf{q}}_0 = \mathbf{J}\dot{\mathbf{q}}_c^+. \tag{22}$$

Therefore $\lambda_c$ is a feasible solution to the QCE-LCP equation. □

**Theorem.** Energy is bounded for QCE-LCP.

*Proof* For the standard LCP with $c_r = 0$ and QCE with $c_r = 1$, two equations can be acquired respectively,

$$\begin{aligned} \mathbf{0} \le \lambda_l \perp \mathbf{J}\mathbf{M}^{-1}\mathbf{J}^T\lambda_l + \mathbf{J}\dot{\mathbf{q}}_0 \ge \mathbf{0} \\ \mathbf{0} \le \lambda_c \perp \mathbf{J}\mathbf{M}^{-1}\mathbf{J}^T\lambda_c + \mathbf{J}\dot{\mathbf{q}}_0 \ge \mathbf{J}\dot{\mathbf{q}}_c^+. \end{aligned} \tag{23}$$

$\lambda_l$ is the solution of LCP and $\lambda_c$ is the solution of QCE. Multiple $1-c_r$ to the first equation and $c_r$ to the second then add them together. Let $\lambda_r = (1-c_r)\lambda_l + c_r\lambda_c$,

$$\mathbf{0} \le \lambda_r \perp \mathbf{J}\mathbf{M}^{-1}\mathbf{J}^T\lambda_r + \mathbf{J}\dot{\mathbf{q}}_0 \ge c_r\mathbf{J}\dot{\mathbf{q}}_c^+. \tag{24}$$

This proves $\lambda_r$ is the solution to QCE-LCP. Let $\dot{\mathbf{q}}_r^+$ be the velocity after adopting $\lambda_r$,

$$\mathbf{M}^{-1}\mathbf{J}^T\lambda_r + \dot{\mathbf{q}}_0 = \dot{\mathbf{q}}_r^+. \tag{25}$$

For $\lambda_l$ and $\lambda_c$, $\dot{\mathbf{q}}_l^+$ and $\dot{\mathbf{q}}_c^+$ are velocities after adopting the two impulses respectively,

$$\begin{aligned} \mathbf{M}^{-1}\mathbf{J}^T\lambda_l + \dot{\mathbf{q}}_l = \dot{\mathbf{q}}_l^+ \\ \mathbf{M}^{-1}\mathbf{J}^T\lambda_c + \dot{\mathbf{q}}_0 = \dot{\mathbf{q}}_c^+. \end{aligned} \tag{26}$$

Again, multiple $1-c_r$ to the first equation and $c_r$ to the second then add them together,

$$\mathbf{M}^{-1}\mathbf{J}^T\lambda_r + \dot{\mathbf{q}}_0 = (1-c_r)\dot{\mathbf{q}}_l^+ + c_r\dot{\mathbf{q}}_c^+ \tag{27}$$

Therefore, $\dot{\mathbf{q}}_r^+ = (1-c_r)\dot{\mathbf{q}}_l^+ + c_r\dot{\mathbf{q}}_c^+$. The kinetic energy $K$ of QCE can be calculated as

$$\begin{aligned} K &= \dot{\mathbf{q}}_r^{+T}\mathbf{M}\dot{\mathbf{q}}_r^+ \\ &= ((1-c_r)\dot{\mathbf{q}}_l^+ + c_r\dot{\mathbf{q}}_c^+)^T\mathbf{M}((1-c_r)\dot{\mathbf{q}}_l^+ + c_r\dot{\mathbf{q}}_c^+) \\ &= (1-c_r)^2\dot{\mathbf{q}}_l^{+T}\mathbf{M}\dot{\mathbf{q}}_l^+ + c_r^2\dot{\mathbf{q}}_c^{+T}\mathbf{M}\dot{\mathbf{q}}_c^+ \\ &\quad + 2c_r(1-c_r)\dot{\mathbf{q}}_l^{+T}\mathbf{M}\dot{\mathbf{q}}_c^+ \\ &\le (1-c_r)^2\dot{\mathbf{q}}_l^{+T}\mathbf{M}\dot{\mathbf{q}}_l^+ + c_r^2\dot{\mathbf{q}}_c^{+T}\mathbf{M}\dot{\mathbf{q}}_c^+ \\ &\quad + c_r(1-c_r)(\dot{\mathbf{q}}_l^{+T}\mathbf{M}\dot{\mathbf{q}}_l^+ + \dot{\mathbf{q}}_c^{+T}\mathbf{M}\dot{\mathbf{q}}_c^+) \\ &= (1-c_r)\dot{\mathbf{q}}_l^{+T}\mathbf{M}\dot{\mathbf{q}}_l^+ + c_r\dot{\mathbf{q}}_c^{+T}\mathbf{M}\dot{\mathbf{q}}_c^+ \end{aligned} \tag{28}$$

It's the proof that the kinetic energy of QCE-LCP is bounded. □